Supplementary Data for "Label-Free Imaging of Lipid-Droplet Intracellular Motion in Early *Drosophila* Embryos Using Femtosecond Stimulated Raman Loss Microscopy", Dou et al.

A. The fSRL Setup

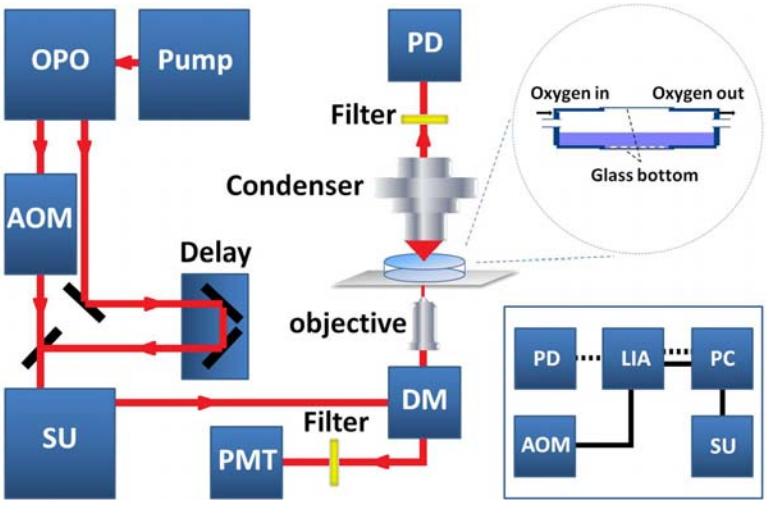

FIGURE S1 *Schematic of the setup for Femtosecond Stimulated Raman Loss Microscopy. A Ti-Sapphire laser pumps an optical parametric oscillator (OPO), generating the pump and Stokes beams. The PD and PMT detect the forward fSRL and backward TPEF signals, respectively, which are then amplified and sent to PC. The top right circle shows the chamber. The bottom right box indicates data flow (dashed lines) and electronic control (solid lines). AOM: acousto-optic modulator. DM: dichroic mirror. LIA: lock-in amplifier. PD: photodiode. PMT: photomultiplier tube. SU: scanning unit.*

B. Photo-Damage Investigation

Our fSRL time-lapse imaging did not lead to a delay of embryonic development and all image frames from phase I to phase III were obtained for a total time span of ~2 hours, the time it takes for *Drosophila* embryogenesis from syncytial blastoderm through gastrulation at 25 °C (1). No photo-damage with membrane blebbing as the indicator was observed during image acquisition (2), and the cephalic and ventral furrows formed at the right times and positions (1). Furthermore, more than half of our imaged embryos hatched within 24 hours at 25 °C (8 out of 12, compared to 7 out 12 from the control group with no imaging operations). The mortality in both groups was likely caused by the preparation steps including bleach dechorionation and immersion in PBS for imaging and mock imaging. These data suggest that fSRL time-lapse imaging causes limited photo-damage to *Drosophila* embryos.

C. Mathematical Modeling of Velocity Jump Processes

We had a total of 12 parameter values used for mathematical modeling in either phase II or phase III (Table S1). These parameter values were obtained by tracking single droplet motion in three individual cortical regions along the apical-basal axis that generally covered the major part of the cortex (Box 1–3 in Fig. S2). To test the sensitivity of the velocity-jump model to variations in these parameter values, we did a parameter sensitivity analysis for both phase II and phase III where each parameter was increased or decreased by 3 percent, 6 percent, 9 percent, and 12 percent (Fig. S3 and S4). Modeling results demonstrate that droplet global distributions in either phase II or phase III are most sensitive to parameter variations of Box 2, which leads to great changes in shape of the droplet distribution along the entire axis. In comparison, parameter variations of Box 1 (or Box 3) greatly change the shape of droplet distribution in its own controlling region, but have relatively small effect on droplet distribution in the other two regions. We suggest that Box 2 plays the central role in controlling droplet net transport. Modeling results also reveal that droplet global distribution is primarily determined by the divergence between apical and basal velocities or turning rates instead of their absolute values (e.g. compare Fig. S3 *E* to S3 *F*, and Fig. S3 *G* to S3 *H*).

To test whether the spatial variation in velocity and turning rate of droplet motion along the apical-basal axis is required for the observed droplet transport system in the embryo, we modeled both phase II and phase III using only one set of velocity and turning rate parameters along the entire apical-basal axis determined by averaging the parameters into one constant. It turns out that parameter variation along the apical-basal axis is important for droplet basal accumulation in phase II but not important in phase III (Fig. S5 for phase II and Fig. S6 for phase III). In phase II, using only Box 2 parameter values for modeling gives the most acceptable droplet distribution changes, but it fails to predict the experimentally observed phenomenon that droplet clearing in phase II is initially more drastic in the apical than in the basal regions. In comparison, this phenomenon is clearly shown by modeling using parameter values in all three boxes. In phase III, however, all model results with the exception of using only Box 2 agree well with that of using parameter values from all three boxes. During phase III, the apical and basal turning rates are nearly equal for all three regions, and the only determinant for droplet net transport is the divergence between the apical and basal velocities. Droplet redistribution during phase III is from the region with smaller parameter values to the region with larger parameter values, which is opposite to the situation in phase II, and the majority of droplets concentrate at the basal-most region at the beginning of phase III. As a result, droplet “jump” may not take effect in this case, rendering the variation in kinetic parameter values of droplet motion along the apical-basal axis an insignificant feature of droplet net transport.

TABLE S1 Velocities and Turning Rates of Lipid-Droplet Motion at Different Apical-Basal Regions, Obtained from Single Particle Tracking Analysis.

(n = number of trajectories)	Velocity (nm/s) Mean ± SEM		Turning Rate (s^{-1}) Mean ± SEM	
	Apical	Basal	Apical	Basal
Phase II				
Box 1 (n = 118)	326 ± 5	305 ± 4	2.61 ± 0.05	2.76 ± 0.05
Box 2 (n = 131)	248 ± 3	232 ± 3	2.11 ± 0.05	2.40 ± 0.05
Box 3 (n = 122)	244 ± 4	219 ± 3	2.30 ± 0.05	2.59 ± 0.05
Phase III				
Box 1 (n = 111)	340 ± 5	323 ± 4	2.39 ± 0.06	2.36 ± 0.06
Box 2 (n = 116)	273 ± 4	265 ± 4	2.20 ± 0.06	2.25 ± 0.06
Box 3 (n = 104)	258 ± 5	238 ± 4	2.31 ± 0.06	2.30 ± 0.06

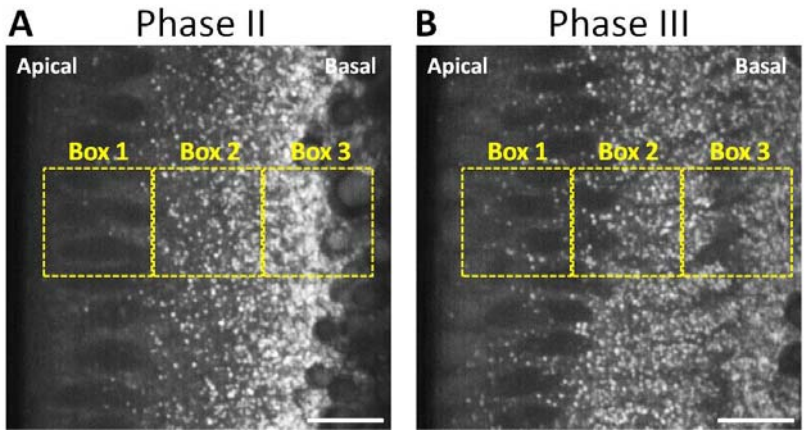

FIGURE S2 *Droplet motion can be characterized by single droplet tracking analysis at different apical-to-basal regions. (A and B) snapshots of the cortex in phase II and phase III. In each snapshot, the imaging regions for droplet tracking correspond to the three yellow boxes, centroids of which are about 15 μm away from each other. Acquisition time, 2 μs per pixel. Bar, 10 μm.*

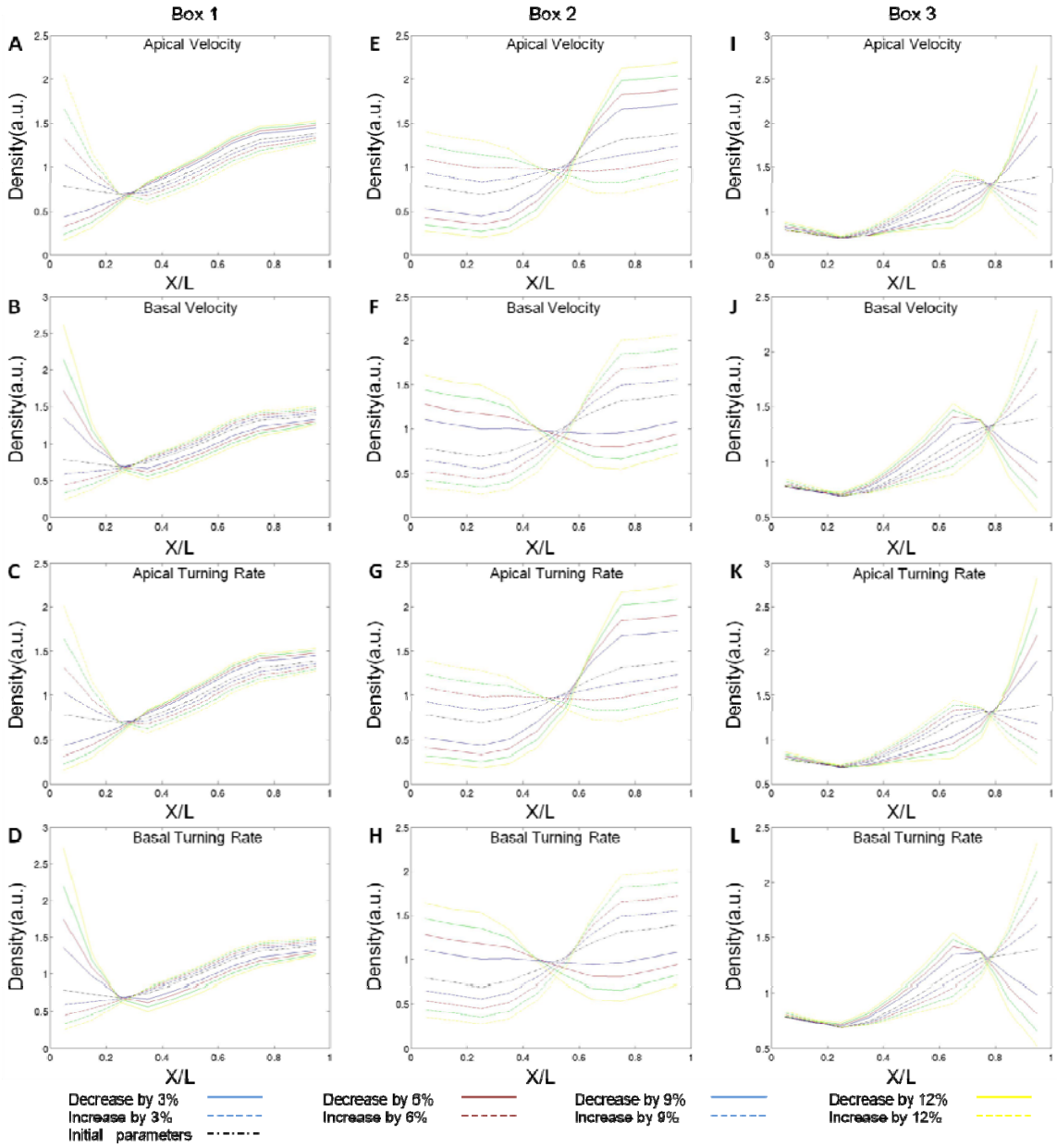

FIGURE S3 *Parameter sensitivity analysis in phase II. Droplet initial distribution (t = 0 min) is uniform as in Fig. 5 A. All droplet density profiles were extracted at t = 20 min. Left to right of the abscissa axis corresponds to the apical-to-basal direction, and its scale is normalized to the width of the embryo cortex L (L = 40 μm).*

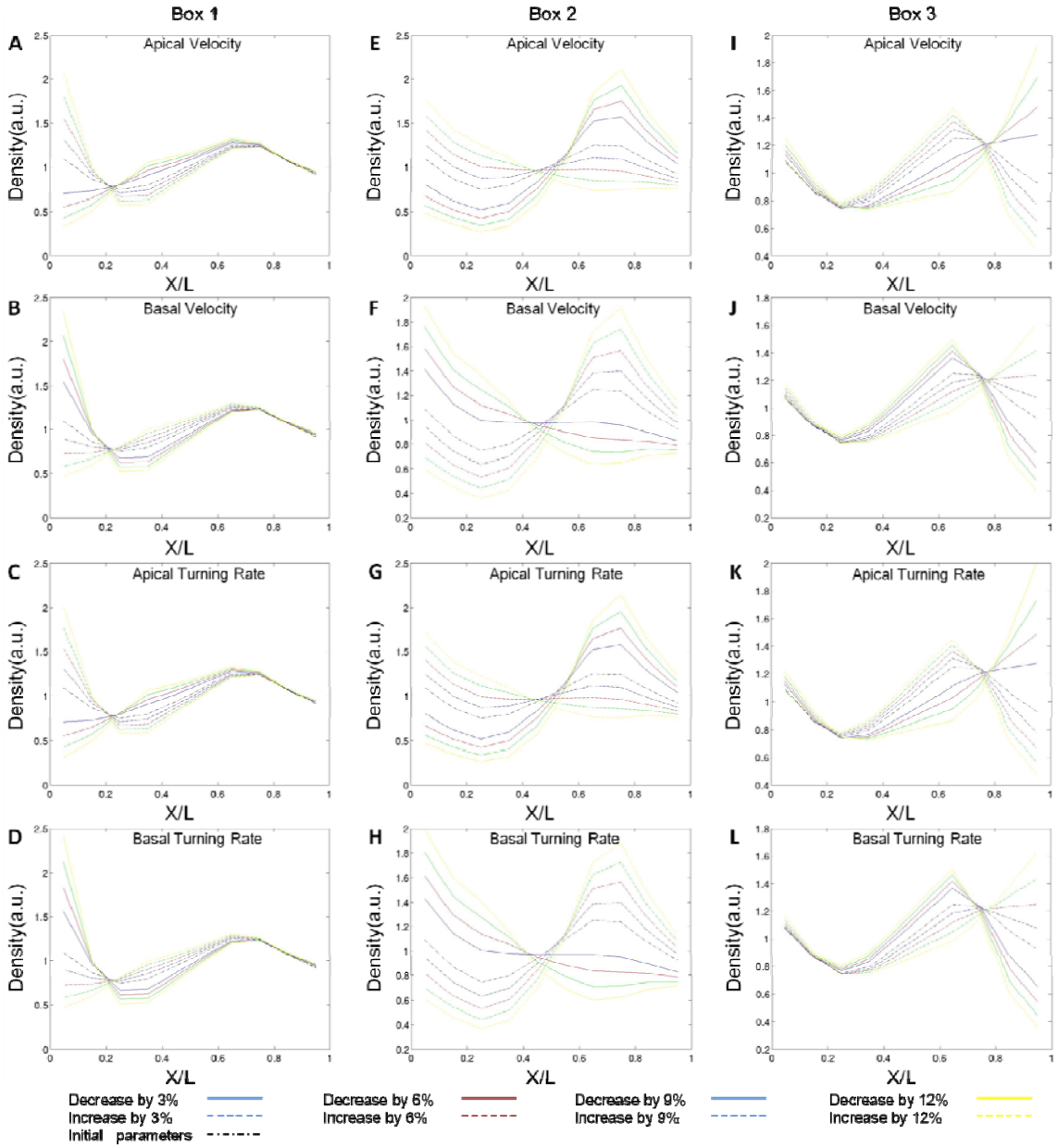

FIGURE S4 *Parameter sensitivity analysis in phase III. Droplet initial distribution (t = 0 min) is that in Fig. 5 F. All droplet density profiles were extracted at t = 10 min.*

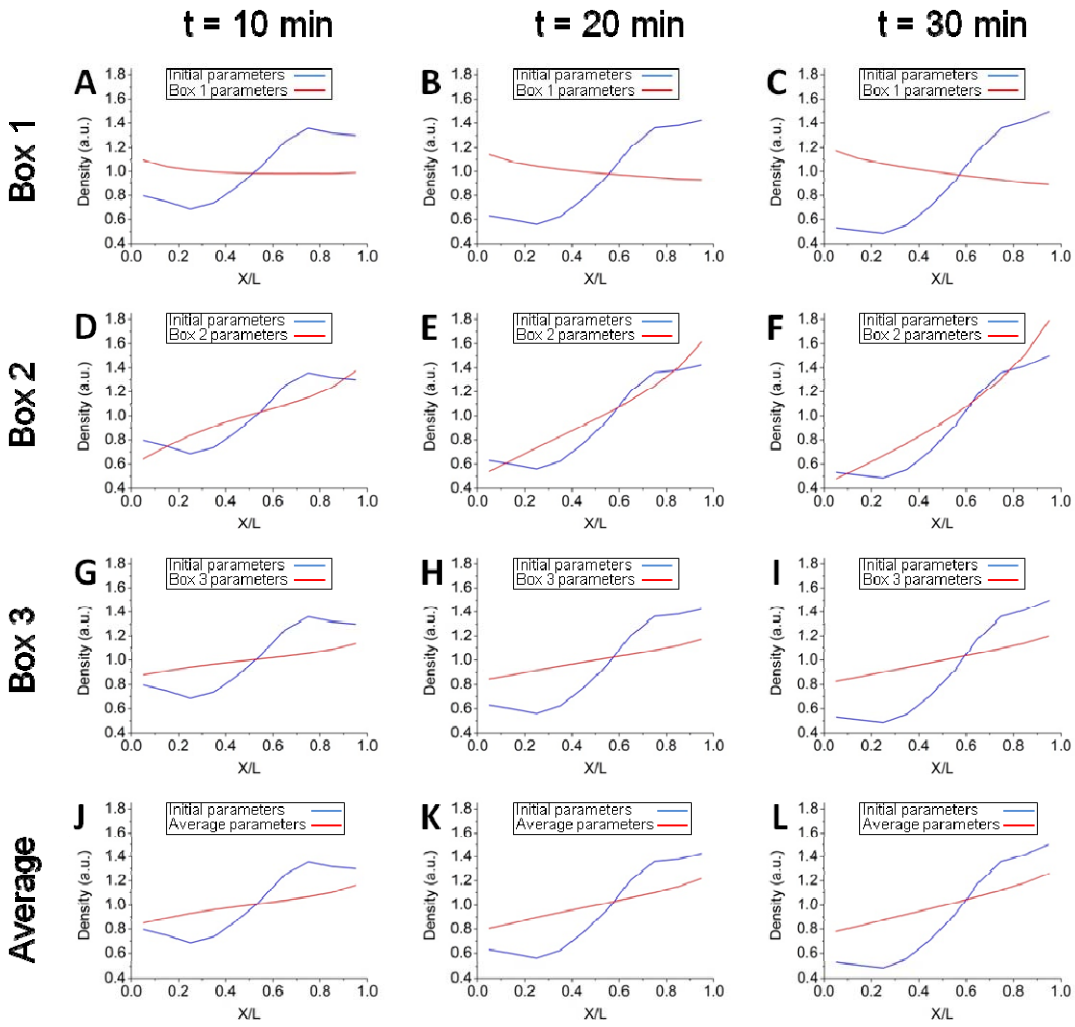

FIGURE S5 *The variation in velocity and turning frequency of droplet motion along the apical-basal axis is an essential feature of droplet basal accumulation in phase II.*

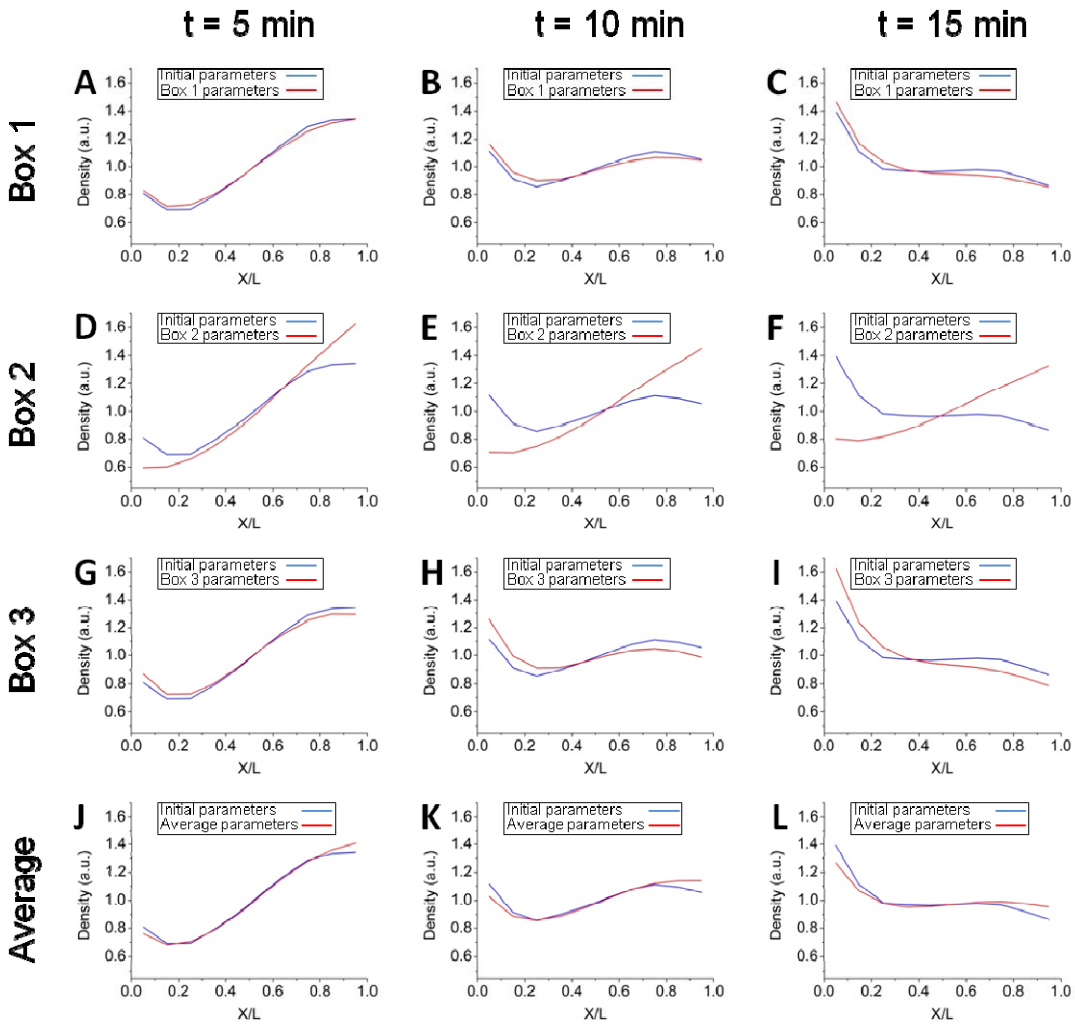

FIGURE S6 *The variation in velocity and turning frequency of droplet motion along the apical-basal axis is not an essential feature of droplet apical redistribution in phase III.*

REFERENCES

1. Foe, V. E., and B. M. Alberts. 1983. Studies of nuclear and cytoplasmic behavior during the five mitotic cycles that precede gastrulation in Drosophila embryogenesis. *J. Cell Sci.* 61:31–70.
2. Zhang, D., M. N. Slipchenko, and J. X. Cheng. 2011. Highly sensitive vibrational imaging by fs pulse stimulated Raman loss. *J. Phys. Chem. Lett.* 2:1248.